

# Encrypted Simultaneous Control of Joint Angle and Stiffness of Antagonistic Pneumatic Artificial Muscle Actuator by Polynomial Approximation

Yuta Takeda, Takaya Shin, Kaoru Teranishi, and Kiminao Kogiso

**Abstract**—This study proposes an encrypted simultaneous control system for an antagonistic pneumatic artificial muscle (PAM) actuator toward developing a cybersecure and flexible actuator. First, a novel simultaneous control system design is considered for the joint angle and stiffness of a PAM actuator in a model-based design approach, facilitating the use of an encrypted control method. The designed controller includes a contraction force model expressed as rational polynomial functions, which makes it difficult to encrypt the controller. To overcome this difficulty, a least absolute shrinkage and selection operator (LASSO)-based polynomial approximation is employed for a rational controller. The resulting polynomial controller is then transformed into a matrix-vector product form, which enables the use of a specific homomorphic encryption scheme to develop an encrypted simultaneous control system for the PAM actuator. Finally, this study quantitatively evaluates the tracking control performance of the original, approximated, and encrypted controllers. The experimental results show that the proposed encrypted controller achieves simultaneous tracking of the joint angle and stiffness with a tracking error of less than 2.7 %.

**Index Terms**—PAM, encrypted control, polynomial-type controller, LASSO, simultaneous control, experimental validation

## I. INTRODUCTION

THE McKibben pneumatic artificial muscle (PAM) was first developed in the 1950s [1]. A PAM is inflated by injecting compressed air into a rubber tube wrapped in a nonstretchable mesh to generate a contraction force. This structure offers several advantages over traditional motors and cylinders, including compact size, lightweight, and flexibility [2], [3]. Because PAMs produce contraction force in a single direction, an antagonistic configuration is typically adopted for practical applications, where two PAMs are arranged in parallel through joints [4]–[12]. This structure facilitates rotational motion and closely mimics human movements [3]. Owing to these benefits, a review paper [13] stated that PAMs have found considerable use in the development of rehabilitation and assistive devices that can be comfortably worn and operated by users. Furthermore, numerous studies have explored stiffness or compliance control [14]–[18] and developed methods of simultaneous control of the joint angle

and stiffness to leverage the potential of PAMs fully [19]–[24]. These active controls enhance safety during contact and collision between robots and humans or their environments while also augmenting the comfort of wearable devices.

Applications that integrate wireless network technology into PAM actuator systems include remote surgical robots [25], remotely operated cranes [26], teleoperation of pneumatic robots [27], and walking-assistive devices [28], [29]. The use of wireless communications enhances the portability of devices and promotes the self-rehabilitation of patients at home. In self-rehabilitation, the monitoring of wearable devices through a network by physical therapists helps prevent injury due to falls. Meanwhile, attention must be paid to the cybersecurity of networked actuator systems. Cyberattack incidents and risk analyses have been reported, such as the falsification of control parameters by Stuxnet to destroy process plants [30], an unmanned aerial vehicle compromised by hijacking video streaming [31], and the compromising of a robot controller [32].

To develop secure PAM actuator systems, networked actuator systems must be equipped with cybersecurity countermeasures. Encrypted control was proposed as a cybersecurity countermeasure for networked control systems in [33] by integrating the homomorphism of a specific public-key encryption scheme into a linear or polynomial-type control system. Encrypted control conceals the control parameters inside the control device and the signals over the communication links, resulting in protection against eavesdropping [33]–[36] and real-time detection of cyberattacks [33], [37], [38]. Encrypted implementation is expected to enhance the cybersecurity of control systems.

However, designing a nonlinear controller that is not a polynomial, such as a rational polynomial or switching controllers, is difficult. A simultaneous control system for the joint angle and stiffness of an antagonistic PAM actuator uses a rational polynomial-type controller [19], [22], [23]. In addition, encrypted proportional-integral (PI) control of the PAM joint angle or torque was considered in [36], and in [39], the implementation of encrypted polynomial controllers was demonstrated, verifying its effectiveness through a numerical toy example. Unfortunately, to the best of our knowledge, no studies have been conducted on encrypting such nonlinear controllers.

The objective of this study is to propose an encrypted simultaneous control system for an antagonistic PAM actuator to develop a cybersecure and flexible actuator. In this study, the

This work was supported by JSPS KAKENHI Grant Numbers JP22H01509 and JP21K19762.

Y. Takeda, K. Teranishi, and K. Kogiso are with the Department of Mechanical and Intelligent Systems Engineering, The University of Electro-Communications, 1-5-1 Chofugaoka, Chofu, Tokyo 1828585, Japan. e-mail: yutataked@uec.ac.jp.

T. Shin is with DAIHEN, Inc.

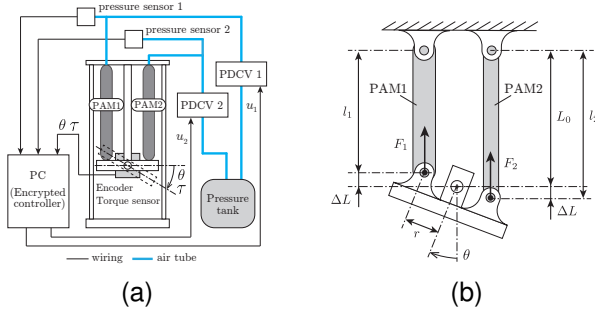


Fig. 1. Antagonistic PAM actuator system considered [40]. (a) Schematic of the entire system and (b) geometric structure of the PAM joint [24].

simultaneous tracking control of the joint angle and stiffness of the antagonistic PAM actuator is considered for a step-like reference. We present a novel model-based nonlinear control system comprising three components: a reference generator, a contraction force estimator, and PI controllers. However, a model-based controller includes specific rational functions, and applying the encrypted control method is challenging. To overcome this difficulty, this study approximates the designed controller as a polynomial-type controller that is friendly to controller encryption. We then quantitatively investigate the effects of polynomial approximation and controller encryption on the control performance to evaluate the developed encrypted control system. Finally, an experimental investigation confirms that the proposed encrypted control system enables simultaneous tracking to the step-like reference within an acceptable tracking error.

This study makes the following main contributions: it is the first to present an encrypted nonlinear control system for simultaneously tracking the joint angle and stiffness of an antagonistic PAM actuator, and it provides a novel form of the contraction force model, which helps reduce the number of approximations that cause control performance degradation throughout the controller encryption procedure.

The remainder of this paper is organized as follows. Section II introduces the antagonistic PAM actuator with a control objective and presents a model-based simultaneous control method for tracking the joint angle and stiffness of the PAM actuator to the reference. Section III discusses the polynomial approximation to acquire a friendly form of the controller to realize the encrypted control. Section IV proposes an encrypted-controlled PAM actuator to maintain the controller and communication secrets and investigates the impact of the secure implementation on the control performance to highlight the effectiveness of the proposed encrypted controller. Finally, Section V concludes the study.

## II. NONLINEAR CONTROL SYSTEM DESIGN FOR ANTAGONISTIC PAM ACTUATOR

This section introduces the antagonistic PAM actuator, its simultaneous control system design, and the numerical evaluation of the control performance of the designed control system.

TABLE I  
EXPERIMENTAL EQUIPMENTS

Name	Specifications
PAM	AirMuscle, Kanda Tsushin Kogyo, Length: 170 mm (be given a 2 kgf mass), Diameter: 0.5 inches
Valve (PDCV)	5/3-way valve, FESTO, a critical frequency of 125 Hz.
Torque sensor	UTM II-10 Nm(R), UNIPULSE, range: $\pm 10$ Nm.
Encoder	UTM II-10 Nm(R), UNIPULSE, Incremental, resolution: 2000 P/R
Pressure sensor	E8F2-B10C, OMRON, Range: 0–1 MPa.
Air compressor	6-25, JUN-AIR, Tank: 25 L; displacement: 60 L/min.
Pressure tank	AST-25G, EARTH MAN, 25 L.
PC	Ubuntu12.04, Xenomai2.6.2.1 Patch, CPU: 3.2 GHz, memory: 8 GB.

### A. Antagonistic PAM Actuator System

Fig. 1(a) shows an antagonistic PAM system. An antagonistic PAM actuator is a joint actuator driven by two PAMs. One side of each PAM is connected by a joint. The system consists of two PAMs, two proportional directional control valves (PDCVs), an air tank, pressure sensors, a torque meter, a rotary encoder, and a control PC. The tank stores compressed air connected to the PDCVs and PAMs using air tubes. The airflow regulated by the PDCVs drives the PAMs, and the joint rotates. The system inputs are the voltage commands to the two PDCVs ( $u_1$  and  $u_2$ ), and the measured values are the joint angle  $\theta$ , torque  $\tau$ , and inner pressure of the PAMs ( $P_1$  and  $P_2$ ). The range of the rotation angle is  $\pm 25$  deg, and the range of the output torque is  $\pm 3.0$  Nm. The sampling period  $T_s$  was set to 20 ms. Table I lists the details of the experimental equipment used.

The control objective considered in this study is to track the joint angle and stiffness of the PAM actuator simultaneously with respect to a given reference. The goal of this study is to develop an encrypted simultaneous tracking control system for the joint angle and stiffness of a PAM actuator to mitigate the control performance degradation caused by secure implementation.

### B. Joint Stiffness

Joint stiffness is an index of the difficulty of a joint rotating against external forces [23], [24]. This study employs the model of joint stiffness presented in [24], following the introduction of the notations of the physical variables regarding the PAM. The geometric relationships of the antagonistic PAM actuator are illustrated in Fig. 1(b), the lengths of the two PAMs,  $l_1$  and  $l_2$ , are respectively given by  $l_1(k) = L_0 - \Delta L(k)$  and  $l_2(k) = L_0 + \Delta L(k)$ , where  $k \in \mathbb{Z}^+ := \{1, 2, \dots\}$  is a step,  $\Delta L(k) \approx r \sin \theta(k)$  is the horizontal displacement of the two PAMs,  $r$  is the radius of the joint, and  $L_0$  is the PAM length when the joint is at the horizontal position. The contraction force of the PAM  $F_i$ ,  $\forall i \in \mathcal{I} := \{1, 2\}$  can be

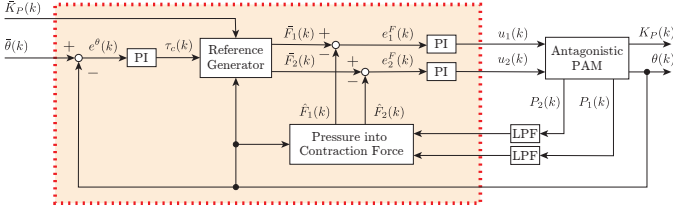


Fig. 2. Block diagram of angle-stiffness control system.

expressed as a function of the inner pressure and length as follows:

$$F_i(l_i(k), P_i(k)) = a_i(l_i(k))P_i(k) + b_i(l_i(k)), \quad \forall i \in \mathcal{I}, \quad (1)$$

with  $a_i(l) = p_i^{a1}l + p_i^{a2}$  and  $b_i(l) = p_i^{b1}l + p_i^{b2}$ ,  $\forall i \in \mathcal{I}$ .

When the joint torque  $\tau$  generated by the two PAMs is given by  $\tau(k) = r \cos \theta(k) (F_1(k) - F_2(k))$ , the joint stiffness  $K_P$  is defined as the partial differentiation of joint torque  $\tau$  by joint angle  $\theta$  as follows [24]:

$$K_P(k) = r \sin \theta(k) (F_1(k) - F_2(k)) + r^2 \cos^2 \theta(k) \left( \frac{F_1(k) - \alpha_1(k)}{l_1(k)} + \frac{F_2(k) - \alpha_2(k)}{l_2(k)} \right), \quad (2)$$

where  $\alpha_i(k) := p_i^{a2}P_i(k) + p_i^{b2}$ ,  $\forall i \in \mathcal{I}$ .

### C. Angle-Stiffness Controller

This study proposes a novel nonlinear controller for the simultaneous control of joint angle and stiffness, which is highlighted in red in Fig. 2, as follows:

$$x(k+1) = A(k; \theta)x(k) + g(k; \zeta), \quad (3a)$$

$$\begin{bmatrix} u_1(k) \\ u_2(k) \end{bmatrix} = C(k; \theta)x(k) + h(k; \zeta) + \begin{bmatrix} \beta_1 \\ \beta_2 \end{bmatrix}, \quad (3b)$$

where  $x \in \mathbb{R}^3$  is the state,  $u_1$  and  $u_2$  are the outputs, and  $\zeta \in \mathbb{R}^5$  is the input, denoted by  $\zeta := [P_1 \ P_2 \ \theta \ \dot{\theta} \ \bar{K}_P]^T$ , where  $P_1$ ,  $P_2$ , and  $\theta$  can be measured by the sensor, and  $\dot{\theta}$  and  $\bar{K}_P$  are the references.  $\beta_1$  and  $\beta_2$  are the bias voltages of each PDCV.  $A(\theta) \in \mathbb{R}^{3 \times 3}$  and  $C(\theta) \in \mathbb{R}^{2 \times 3}$  are time-varying,  $\theta$ -dependent coefficients, and  $g: \mathbb{R}^5 \rightarrow \mathbb{R}^3$  and  $f: \mathbb{R}^5 \rightarrow \mathbb{R}^3$  are nonlinear functions of  $\zeta$ . The coefficients and nonlinear functions are clarified after introducing a reference generator, pressure into the contraction force, and PI controllers, which are components of the proposed controller and are explained as follows.

1) *Reference Generator*: The reference generator outputs the reference signals of the contraction force for two PAMs, denoted as  $\bar{F}_1$  and  $\bar{F}_2$ , taking the measured joint angle  $\theta$ , computed torque command  $\tau_c$ , and the given reference of joint stiffness  $\bar{K}_P$  as inputs. Using [24],  $\bar{F}_1$  and  $\bar{F}_2$  are expressed as rational polynomial functions of the inputs  $\theta$ ,  $\tau_c$ , and  $\bar{K}_P$ :

$$\bar{F}_1(k) = \frac{1}{r^2 \cos^2 \theta(k)} \frac{l_1(k)l_2(k)}{l_1(k) + l_2(k)} \left[ \bar{K}_P(k) + \left( \frac{r \cos \theta(k)}{l_2(k)} - \tan \theta(k) \right) \tau_c(k) - r^2 \cos^2 \theta(k) \left( \frac{\alpha_1(k)}{l_1(k)} + \frac{\alpha_2(k)}{l_2(k)} \right) \right], \quad (4a)$$

$$\bar{F}_2(k) = \bar{F}_1(k) - \frac{\tau_c(k)}{r \cos \theta(k)}. \quad (4b)$$

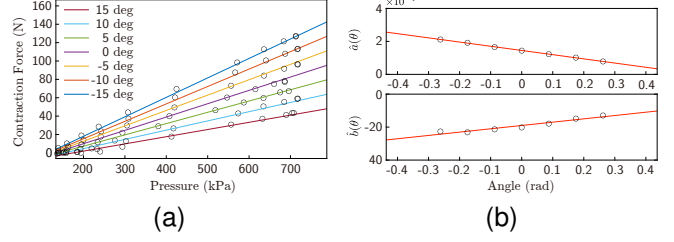


Fig. 3. Fitting result of the  $\theta$ -dependent model (5) for capturing static characteristics with regard to  $P$ ,  $F$ , and  $\theta$  of the PAMs. (a)  $P$ - $F$  relationship of the PAM. (b)  $\hat{a}$ - $\theta$  and  $\hat{b}$ - $\theta$  relationships of the PAM.

2) *Pressure into Contraction Force*: The pressure-to-contraction force block shown in Fig. 2 estimates the contraction force of the PAM by using the following experimental polynomial function of the inner pressure and measured joint angle:

$$\hat{F}_i(\theta(k), P_i(k)) = \hat{a}_i(\theta(k))P_i(k) + \hat{b}_i(\theta(k)), \quad (5a)$$

$$\hat{a}_i(\theta) = p_i^{\hat{a}1}\theta + p_i^{\hat{a}2}, \quad \hat{b}_i(\theta) = p_i^{\hat{b}1}\theta + p_i^{\hat{b}2}, \quad (5b)$$

where  $\hat{F}_i$ ,  $\hat{a}_i$ , and  $\hat{b}_i$ ,  $\forall i \in \mathcal{I}$ , are an estimate of the PAM contraction force and the coefficients of (5a), respectively.

A reason for introducing the contraction force model (5) in addition to (1) is to reduce the number of approximation, which will facilitate the discussion in Section III. Model (1) involves a nonlinear term  $\sin \theta$ , which requires the approximation process to be a polynomial. On the other hand, the model (5) is a polynomial of  $\theta$  and captures a static relationship between the angle and the contraction force. Indeed, the fitting results of (5) are shown in Fig. 3. In Fig. 3(a), the black circles represent experimentally measured data, and the colored lines represent fitting results using (5) for each angle. In this case, the coefficients (5b) for each angle correspond to Fig. 3(b), where the black circles represent the coefficients corresponding to the colored lines in Fig. 3(a). The fitting test confirms that the  $\theta$ -dependent model (5) is valid.

3) *PI Controller*: The proposed controller includes two types of PI controllers to compensate for errors in the joint angle and the contraction force. The controller for the joint angle uses a feedback error between  $\bar{\theta}$  and  $\theta$ , denoted by  $e^\theta := \bar{\theta} - \theta$ , to compute the command torque  $\tau_c$ , as follows:

$$\begin{bmatrix} x^\theta(k+1) \\ \tau_c(k) \end{bmatrix} = \begin{bmatrix} 1 & T_s \\ G_1^\theta & G_P^\theta \end{bmatrix} \begin{bmatrix} x^\theta(k) \\ e^\theta(k) \end{bmatrix}, \quad (6)$$

where  $x^\theta$  is the state and  $G_P^\theta$  and  $G_1^\theta$  are the proportional and integral gains, respectively.

Regarding the contraction force controller, the outputs of the reference generator,  $\bar{F}_1$  and  $\bar{F}_2$ , are compared with the estimated forces  $\hat{F}_1$  and  $\hat{F}_2$  computed by (5), respectively. The resulting errors are fed to the PI controllers to generate the control input voltages  $u_1$  and  $u_2$  for each PDCV. The controllers are given as follows:

$$\begin{bmatrix} x_i^F(k+1) \\ u_i(k) \end{bmatrix} = \begin{bmatrix} 1 & T_s & 0 \\ G_1^F & G_P^F & 1 \end{bmatrix} \begin{bmatrix} x_i^F(k) \\ e_i^F(k) \\ \beta_i \end{bmatrix}, \quad \forall i \in \mathcal{I}, \quad (7)$$

$$A(k; \theta) = \begin{bmatrix} 1 & 0 & 0 \\ \frac{T_s G_1^\theta l_1(k) l_2(k)}{r^2 (l_1(k) + l_2(k)) \cos^2 \theta(k)} \left( \frac{r \cos \theta(k)}{l_2(k)} - \tan \theta(k) \right) & 1 & 0 \\ T_s G_1^\theta \left\{ \frac{l_1(k) l_2(k)}{r^2 (l_1(k) + l_2(k)) \cos^2 \theta(k)} \left( \frac{r \cos \theta(k)}{l_2(k)} - \tan \theta(k) \right) - \frac{1}{r \cos \theta(k)} \right\} & 0 & 1 \end{bmatrix}, \quad g(k; \zeta) = T_s \begin{bmatrix} \bar{\theta}(k) - \theta(k) \\ h_1(k; \zeta) \\ h_2(k; \zeta) \end{bmatrix}, \quad (8a)$$

$$C(k; \theta) = \begin{bmatrix} G_P^F G_1^\theta \left\{ \frac{l_1(k) l_2(k)}{r^2 (l_1(k) + l_2(k)) \cos^2 \theta(k)} \left( \frac{r \cos \theta(k)}{l_2(k)} - \tan \theta(k) \right) - \frac{1}{r \cos \theta(k)} \right\} & G_I^F & 0 \\ G_P^F G_1^\theta \left\{ \frac{l_1(k) l_2(k)}{r^2 (l_1(k) + l_2(k)) \cos^2 \theta(k)} \left( \frac{r \cos \theta(k)}{l_2(k)} - \tan \theta(k) \right) - \frac{1}{r \cos \theta(k)} \right\} & 0 & G_I^F \end{bmatrix}, \quad h(k; \zeta) = G_P^F \begin{bmatrix} h_1(k; \zeta) \\ h_2(k; \zeta) \end{bmatrix}, \quad (8b)$$

$$h_1(k; \zeta) := \frac{l_1(k) l_2(k)}{l_1(k) + l_2(k)} \left[ \frac{1}{r^2 \cos^2 \theta(k)} \left\{ -\bar{K}_P(k) + G_P^\theta \left( \frac{r \cos \theta(k)}{l_2(k)} - \tan \theta(k) \right) (\bar{\theta}(k) - \theta(k)) \right\} + \frac{\alpha_1(k)}{l_1(k)} + \frac{\alpha_2(k)}{l_2(k)} \right] - \hat{a}_1 P_1(k) - \hat{b}_1, \quad (8c)$$

$$h_2(k; \zeta) := \frac{l_1(k) l_2(k)}{l_1(k) + l_2(k)} \left[ \frac{1}{r^2 \cos^2 \theta(k)} \left\{ -\bar{K}_P(k) + G_P^\theta \left( \frac{r \cos \theta(k)}{l_2(k)} - \tan \theta(k) - \frac{l_1(k) + l_2(k)}{l_1(k) l_2(k)} r \cos \theta(k) \right) (\bar{\theta}(k) - \theta(k)) \right\} + \frac{\alpha_1(k)}{l_1(k)} + \frac{\alpha_2(k)}{l_2(k)} \right] - \hat{a}_2 P_2(k) - \hat{b}_2, \quad (8d)$$

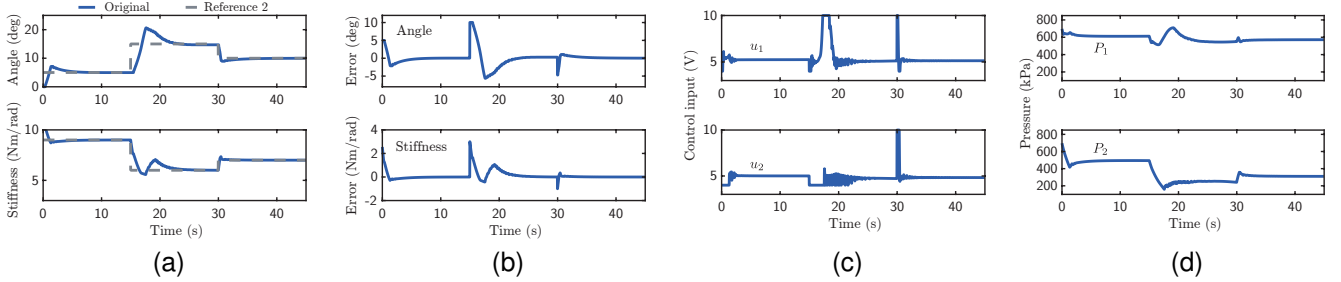


Fig. 4. Simulation results of the original simultaneous control of joint angle and stiffness for Reference 2. (a) Joint angle and stiffness, (b) tracking errors of the joint angle and stiffness, (c) control inputs to the valve, and (d) inner pressure of each PAM.

where  $x_i^F, \forall i \in \mathcal{I}$ , is the state of the  $i$ -th controller,  $e_i^F := \bar{F}_i - \hat{F}_i, \forall i \in \mathcal{I}$ , is the error in the contraction force of the  $i$ th PAM,  $G_P^F$  and  $G_I^F$  are the proportional and integral gains, respectively, and the gains are common between the controllers. Additionally, we set  $\beta_i = 5.0, \forall i \in \mathcal{I}$ .

Consequently, defining the controller state by  $x := [x^\theta \ x_1^F \ x_2^F]^\top$  and eliminating  $\tau_c, e^\theta, e_i^F, \bar{F}_i$ , and  $\hat{F}_i, \forall i \in \mathcal{I}$  from (4)–(7) results in the nonlinear controller (3) with the coefficients and functions in (8).

#### D. Numerical Verification

This section presents the numerical simulations conducted to evaluate the proposed nonlinear controller in terms of the control performance with respect to simultaneous angle-stiffness control. For the simulations, we used the following state-space model of an antagonistic PAM system [40]:  $x_p(k+1) = f_\sigma(x_p(k), u(k))$  if  $x_p(k) \in \mathcal{X}_\sigma$  holds,  $y(k) = h_p(x_p(k))$ , where  $u := [u_1 \ u_2]^\top \in [0, 10]^2 \subset \mathbb{R}^2$  is the input voltages (V) to the two PDCVs, the state variable is  $x_p := [\theta \ \dot{\theta} \ P_1 \ P_2]^\top \in \mathbb{R}^4$ , and the output variable is  $y := [\theta \ P_1 \ P_2 \ K_P]^\top \in \mathbb{R}^4$ , in which a set of allowable absolute pressures (kPa) is determined by the specification of the PAMs, i.e.,  $P_1, P_2 \in [200, 750]$ ,  $f_\sigma : \mathbb{R}^4 \rightarrow \mathbb{R}^4$  is a nonlinear function with 18 subsystems, and it switches

according to if-then rules,  $\mathcal{X}_\sigma := \{x_p \in \mathbb{R}^4 \mid \Psi_\sigma(x_p) > 0\}$  is the state set, where  $\sigma \in \{1, 2, \dots, 18\}$  is the index of the subsystem,  $\Psi_\sigma(x_p)$  is a function derived from the modes in the form of if-then rules, and the function  $h_p : \mathbb{R}^4 \rightarrow \mathbb{R}^4$  is an observation equation.

We considered two types of references of the joint angle and stiffness. Reference 1 was set to

$$(\bar{\theta}(k), \bar{K}_P(k)) = \begin{cases} (10, 8) & \text{if } 0 \leq T_s k < 15, \\ (10, 6) & \text{if } 15 \leq T_s k < 30, \\ (10, 4) & \text{if } 30 \leq T_s k < 45, \end{cases}$$

and Reference 2 was set to

$$(\bar{\theta}(k), \bar{K}_P(k)) = \begin{cases} (5, 9) & \text{if } 0 \leq T_s k < 15, \\ (15, 6) & \text{if } 15 \leq T_s k < 30, \\ (10, 7) & \text{if } 30 \leq T_s k < 45. \end{cases}$$

The parameters of the PI controllers in (6) and (7) were determined by trial and error, resulting in  $G_P^\theta = 0.25$ ,  $G_I^\theta = 0.13$ ,  $G_P^F = 0.088$ , and  $G_I^F = 0.08$ . The initial voltage commands  $u_1(0) = u_2(0) = 5.5$  were given before the start of the control, and the control was started after sufficient time had elapsed. Additionally, note that the simulation and experimental results regarding Reference 1 have been omitted, and the results are discussed in Section IV-C owing to page limitations.

The simulation results are provided in Fig. 4, where (a) shows the time response of the joint angle and stiffness, (b) presents the tracking errors of the joint angle and stiffness, (c) depicts the control inputs to the valve, and (d) shows the inner pressure of each PAM. Figs. 4(a)(b) confirm that the joint angle and stiffness track the reference in a steady state. In this case, the input voltage oscillates in a transient state, as shown in Fig. 4(c). The operating pressure behavior is shown in Fig. 4(d). These results confirm that the proposed nonlinear controller achieves simultaneous tracking control of the joint angle and stiffness of the PAM actuator system.

However, the coefficients and input functions in the proposed controller are rational functions, which makes them difficult to implement in a controller device in an encrypted control fashion. Therefore, in the next section, we consider polynomial approximation of the proposed controller.

*Remark 1:* The novelty of the proposed controller (3) is the use of the  $\theta$ -dependent contraction force model (5), compared to the UKF-based simultaneous controller [24]. The UKF-based controller involving fluid dynamics [24] and sliding mode controllers [20], [21] include an if-then rule; therefore, obtaining an alternative controller in a polynomial is difficult. Meanwhile, the nonlinear controllers proposed in [19], [22], [23] can be applied to a polynomial approximation, whereas costly force sensors are required to measure the contraction force.

### III. POLYNOMIAL APPROXIMATION OF THE CONTROLLER

This section presents the approximation of the proposed controller into polynomial functions and investigates the impact of the approximation on the response of the experimental PAM control system.

#### A. Controller Approximation

This study uses one- and two-variable functions to approximate the reference generator (4) in polynomials because only the reference generator is a rational function. By introducing five functions denoted by  $f_1, \dots, f_5$ , let the rational functions (4) be rewritten as follows:

$$\bar{F}_1(k) = f_1(k; \theta, \bar{K}_P) + f_2(k; \theta)\tau_c(k) + f_3(k; \theta, P_1) + f_4(k; \theta, P_2),$$

$$\bar{F}_2(k) = \bar{F}_1(k) + f_5(k; \theta)\tau_c(k),$$

where

$$\begin{aligned} f_1(k; \theta, \bar{K}_P) &:= -\frac{l_1(k)l_2(k)\bar{K}_P(k)}{r^2(l_1(k) + l_2(k))\cos^2\theta(k)}, \\ f_2(k; \theta) &:= \frac{l_1(k)l_2(k)}{r^2(l_1(k) + l_2(k))\cos^2\theta(k)} \left( \frac{r\cos\theta(k)}{l_2(k)} - \tan\theta(k) \right), \\ f_3(k; \theta, P_1) &:= \frac{\alpha_1(P_1(k))l_2(k)}{l_1(k) + l_2(k)}, \\ f_4(k; \theta, P_2) &:= \frac{\alpha_2(P_2(k))l_1(k)}{l_1(k) + l_2(k)}, \\ f_5(k; \theta) &:= -\frac{1}{r\cos\theta(k)}. \end{aligned}$$

For the five functions, we used the LASSO-based polynomial approximation [41] and manually removed coefficients with relatively small values, which resulted in the following approximated functions:

$$\begin{aligned} f_1(k; \theta, \bar{K}_P) &\approx w_1\bar{K}_P(k) + w_2\theta^2(k)\bar{K}_P(k) + w_3 =: \hat{f}_1, \\ f_2(k; \theta) &\approx w_4\theta(k) + w_5\theta^2(k) + w_6 =: \hat{f}_2, \\ f_3(k; \theta, P_1) &\approx w_7P_1(k) + w_8\theta(k)P_1(k) + \\ &\quad w_s\theta(k)P_1^2(k) + w_9, \\ &\approx w_7P_1(k) + w_8\theta(k)P_1(k) + w_9 =: \hat{f}_3, \\ f_4(k; \theta, P_2) &\approx w_{10}P_2(k) + w_{11}\theta(k)P_2(k) + w_{12} =: \hat{f}_4, \\ f_5(k; \theta) &\approx w_{13}\theta^2(k) + w_{14} =: \hat{f}_5, \end{aligned}$$

where  $w_i, \forall i \in \{1, 2, \dots, 14\}$  and  $w_s$  are coefficients of approximated polynomials  $\hat{f}_j, \forall j \in \{1, 2, \dots, 5\}$ , and their values are listed in TABLE II, where the regularization parameter of LASSO was set to 1.0.  $\hat{f}_2$  and  $\hat{f}_5$  are cubic polynomials in  $\theta$ , and the other functions are cubic in both arguments. Furthermore,  $w_s$  of  $\hat{f}_3$  resulted in a nonzero term, but it was significantly small compared to the other coefficients; thus we removed  $w_s$ .

Consequently, we obtained the polynomial controller in (3) by using the approximated coefficient matrices and functions specified below,

$$A(k; \theta) \approx \begin{bmatrix} 1 & 0 & 0 \\ T_s G_1^\theta \hat{f}_2(k; \theta) & 1 & 0 \\ T_s G_1^\theta (\hat{f}_2(k; \theta) + \hat{f}_5(k; \theta)) & 0 & 1 \end{bmatrix}, \quad (9a)$$

$$C(k; \theta) \approx \begin{bmatrix} G_P^F G_1^\theta \hat{f}_2(k; \theta) & G_1^F & 0 \\ G_P^F G_1^\theta (\hat{f}_2(k; \theta) + \hat{f}_5(k; \theta)) & 0 & G_1^F \end{bmatrix}, \quad (9b)$$

$$h_1(k; \zeta) \approx \hat{f}_1(k; \theta, \bar{K}_P) + G_P^\theta \hat{f}_2(k; \theta)(\bar{\theta}(k) - \theta(k)) + \hat{f}_3(k; \theta, P_1) + \hat{f}_4(k; \theta, P_2) - \hat{a}_1 P_1(k) - \hat{b}_1, \quad (9c)$$

$$h_2(k; \zeta) \approx \hat{f}_1(k; \theta, \bar{K}_P) + \hat{f}_3(k; \theta, P_1) + \hat{f}_4(k; \theta, P_2) + G_P^\theta (\hat{f}_2(k; \theta) + \hat{f}_5(k; \theta))(\bar{\theta}(k) - \theta(k)) - \hat{a}_2 P_2(k) - \hat{b}_2. \quad (9d)$$

#### B. Evaluation of Approximation Impacts

The impact of the controller approximation on the control performance is evaluated by comparing the experimental time responses of the control systems using the original controller (8) and the approximated controller (9). The scenarios of the control experiments are simultaneous tracking control of the joint angle and stiffness with and without a load. The references of the joint angle and stiffness set in the experiments are the same as those employed in the simulations. Before the start of the control, an initial voltage command  $u_1(0) = u_2(0) = 5.5$  were provided, and the control was initiated after sufficient time had elapsed.

The experimental results for the original and approximated controllers without a load are shown in Fig. 5. In this figure, the blue and red lines indicate the results of the original and approximated control systems, respectively, and their meanings are the same as those in Fig. 4. Figs. 5(a)(b) confirm that the

TABLE II  
LIST OF PARAMETERS IN APPROXIMATED CONTROLLER

$w_1$	-61.7	$p_1^{a_1}$	$7.05 \times 10^{-3}$
$w_2$	$-1.89 \times 10^{-2}$	$p_1^{b_2}$	$-1.02 \times 10^{-4}$
$w_3$	-1.58	$p_1^{b_1}$	$-5.57 \times 10^2$
$w_4$	13.6	$p_1^{b_2}$	72.86
$w_5$	-1.24	$p_2^{a_1}$	$6.42 \times 10^3$
$w_6$	$1.73 \times 10^{-3}$	$p_2^{b_2}$	$-9.18 \times 10^{-4}$
$w_7$	$-5.12 \times 10^{-1}$	$p_2^{b_1}$	$-1.98 \times 10^2$
$w_8$	$-1.18 \times 10^{-3}$	$p_2^{b_2}$	15.75
$w_s$	$-5.76 \times 10^{-7}$	$p_1^{a_1}$	$-2.55 \times 10^{-4}$
$w_9$	36.5	$p_1^{b_2}$	$1.45 \times 10^{-4}$
$w_{10}$	$-4.31 \times 10^{-1}$	$p_1^{b_1}$	20.14
$w_{11}$	$1.54 \times 10^{-3}$	$p_1^{b_2}$	-19.01
$w_{12}$	-9.35	$p_2^{a_1}$	$2.18 \times 10^{-4}$
$w_{13}$	-27.3	$p_2^{a_2}$	$1.45 \times 10^{-4}$
$w_{14}$	$-3.92 \times 10^{-3}$	$p_2^{b_1}$	1.35
$G_P^\theta$	1.3	$p_2^{b_2}$	-18.67
$G_I^\theta$	$2.43 \times 10^{-1}$	$G_I^F$	$2.50 \times 10^{-2}$
$G_P^F$	$8.80 \times 10^{-2}$		

angle and stiffness track the reference in the steady state and that sufficient control performance is maintained. Additionally, the improvement in transient-response control performance is believed to be due to the impacts of quantization; however, the details have not been clearly established. Figs. 5(c)(d) observe that the experimental results of the original and approximated controllers exhibit similar behavior in the steady state.

Moreover, we conducted a control experiment in which a 1.5 kg load was hung from the left side of the joint before starting control to evaluate the impact of the approximation. The experimental results of the loads are shown in Fig. 6, where the line colors in each figure are the same as those in Fig. 5. Figs. 6(a)(b) confirm that the angle and stiffness track the reference in the steady state. Good control tracking causes the controller to compensate for the impact of the load, which can be observed as a difference of approximately 50 kPa over the steps between the responses of the inner pressures, as shown in Figs. 5(d) and 6(d). Similarly, Fig. 6(c) demonstrates that the experimental results of the two controllers exhibit similar behaviors in the steady state, respectively.

The experimental results confirm that the approximated controller achieves almost the same control performance as the original controller, implying that the impact of the controller approximation is negligible. Therefore, the original controller can be replaced with an approximated controller that is adequate for secure implementation.

#### IV. SECURE PAM ACTUATOR WITH ENCRYPTED POLYNOMIAL-TYPE CONTROLLER

This section describes the encrypted control of the joint angle and the stiffness of an antagonistic PAM actuator system.

##### A. Secure Implementation

The controller encryption method in [33] can be applied to a linear controller in a matrix-vector product form. Hence, we consider to transform our proposed polynomial controller

into a product of matrix and vector. In this study, by defining a vector of monomials as  $\xi \in \mathbb{R}^{18}$ , the polynomial controller (3) with the coefficients and functions (9) can be transformed into the following matrix-vector multiplication:

$$\psi(k) = \Phi \xi(k), \quad \forall k \in \mathbb{Z}^+, \quad (10)$$

with

$$\xi := [\bar{K}_P \quad \bar{K}_P \theta^2 \quad \bar{\theta} \quad \theta \quad x^\theta \quad \bar{\theta} \theta \quad \theta^2 \quad x^\theta \theta \quad \bar{\theta} \theta^2 \quad \theta^3 \quad x^\theta \theta^2 \quad P_1 \quad \theta P_1 \quad P_2 \quad \theta P_2 \quad 1 \quad x^{F_1} \quad x^{F_2}]^T,$$

$$\psi(k) := [x^\theta(k+1) \quad x_1^F(k+1) \quad x_2^F(k+1) \quad u_1(k) \quad u_2(k)]^T,$$

where  $\xi$  and  $\psi \in \mathbb{R}^5$  are the input and output of the encrypted controller, respectively. The coefficient matrix  $\Phi \in \mathbb{R}^{5 \times 18}$  is given as follows:

$$\Phi = \begin{bmatrix} 0 & 0 & T_s & -T_s & 1 & 0 \\ T_s w_1 & T_s w_2 & T_s \phi_3 & T_s \phi_4 & T_s \phi_5 & T_s \phi_6 \\ T_s w_1 & T_s w_2 & T_s \nu_3 & T_s \nu_4 & T_s \nu_5 & T_s \nu_6 \\ G_P^F w_1 & G_P^F w_2 & G_P^F \phi_3 & G_P^F \phi_4 & G_P^F \phi_5 & G_P^F \phi_6 \\ G_P^F w_1 & G_P^F w_2 & G_P^F \nu_3 & G_P^F \nu_4 & G_P^F \nu_5 & G_P^F \nu_6 \\ 0 & 0 & 0 & 0 & 0 & 0 \\ T_s \phi_7 & T_s \phi_8 & T_s \phi_9 & T_s \phi_{10} & T_s \phi_{11} & T_s \phi_{12} \\ G_P^F \phi_7 & G_P^F \phi_8 & G_P^F \phi_9 & G_P^F \phi_{10} & G_P^F \phi_{11} & T_s \nu_{12} \\ G_P^F \phi_7 & G_P^F \phi_8 & G_P^F \phi_9 & G_P^F \phi_{10} & G_P^F \phi_{11} & G_P^F \phi_{12} \\ G_P^F \nu_7 & G_P^F \nu_8 & G_P^F \nu_9 & G_P^F \nu_{10} & G_P^F \nu_{11} & G_P^F \nu_{12} \\ 0 & 0 & 0 & 0 & 0 & 0 \\ T_s \phi_{13} & T_s \phi_{14} & T_s \phi_{15} & T_s \phi_{16} & 1 & 0 \\ T_s \nu_{13} & T_s \nu_{14} & T_s \nu_{15} & T_s \nu_{16} & 0 & 1 \\ G_P^F \phi_{13} & G_P^F \phi_{14} & G_P^F \phi_{15} & G_P^F \phi_{16} + \beta_1 & G_I^F & 0 \\ G_P^F \nu_{13} & G_P^F \nu_{14} & G_P^F \nu_{15} & G_P^F \nu_{16} + \beta_2 & 0 & G_I^F \end{bmatrix},$$

where  $\phi_3 := w_4 G_P^\theta$ ,  $\phi_4 := -p_1^{b_1} - w_4 G_P^\theta$ ,  $\phi_5 := w_4 G_I^\theta$ ,  $\phi_6 := w_5 G_P^\theta$ ,  $\phi_7 := -w_5 G_P^\theta$ ,  $\phi_8 := w_5 G_I^\theta$ ,  $\phi_9 := w_6 G_P^\theta$ ,  $\phi_{10} := -w_6 G_P^\theta$ ,  $\phi_{11} := w_6 G_I^\theta$ ,  $\phi_{12} := w_7 - p_2^{a_1}$ ,  $\phi_{13} := w_8 - p_1^{a_1}$ ,  $\phi_{14} := w_{10}$ ,  $\phi_{15} := w_{11}$ ,  $\phi_{16} := w_3 + w_9 + w_{12} - p_2^{b_1}$ ,  $\nu_3 := (w_4 + w_{13}) G_P^\theta$ ,  $\nu_4 := -p_1^{b_2} - (w_4 + w_{13}) G_P^\theta$ ,  $\nu_5 := (w_4 + w_{13}) G_I^\theta$ ,  $\nu_6 := w_5 G_P^\theta$ ,  $\nu_7 := -w_5 G_P^\theta$ ,  $\nu_8 := w_5 G_I^\theta$ ,  $\nu_9 := (w_6 + w_{14}) G_P^\theta$ ,  $\nu_{10} := -(w_6 + w_{14}) G_P^\theta$ ,  $\nu_{11} := (w_6 + w_{14}) G_I^\theta$ ,  $\nu_{12} := w_7$ ,  $\nu_{13} := w_8$ ,  $\nu_{14} := w_{10} - p_2^{a_2}$ ,  $\nu_{15} := w_{11} - p_1^{a_2}$ , and  $\nu_{16} := w_3 + w_9 + w_{12} - p_2^{b_2}$ . The augmented formulation of the controller (10) is a linear operation; thus, the same procedure for encrypting a linear controller is applied to encrypt the controller, as described in [36]. The configuration of the control system is illustrated in Fig. 7, where the controller input  $\xi$  is generated by the reference signals, measurements, and states of the PI controllers. The input  $\xi$  is encrypted by using an ElGamal encryption scheme in the Enc block. The encrypted controller Enc( $\Phi$ ) conducts multiplicative homomorphic operations, and Dec<sup>+</sup> extracts the plaintext states and control inputs to each PDCV. For the notations regarding the encryption scheme, please refer to [33].

##### B. Experimental Validation

This section verifies the encrypted control system by comparing the experimental results obtained using the encrypted and original control systems. A key length of 64 bit was



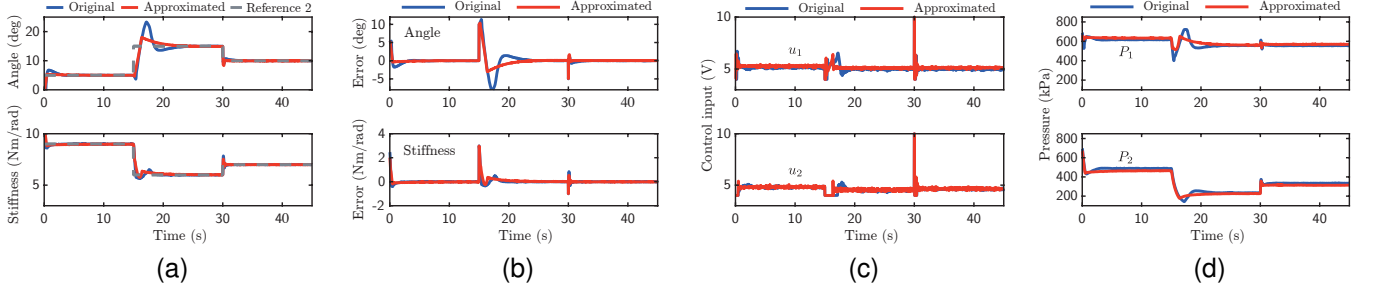


Fig. 5. Comparison of experimental results of original and approximated polynomial load-free controls of joint angle and stiffness for Reference 2. (a) Joint angle and stiffness, (b) tracking errors of the joint angle and stiffness, (c) control inputs to the valve, and (d) inner pressure of each PAM.

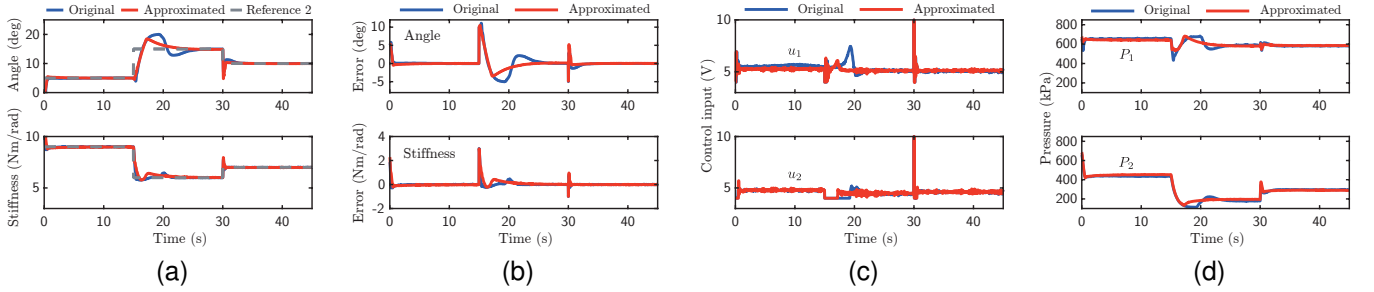


Fig. 6. Comparison of experimental results of original and approximated polynomial controls with load for Reference 2. (a) Joint angle and stiffness, (b) Tracking errors of the joint angle and stiffness, (c) Control inputs to the valve, and (d) Inner pressure of each PAM.

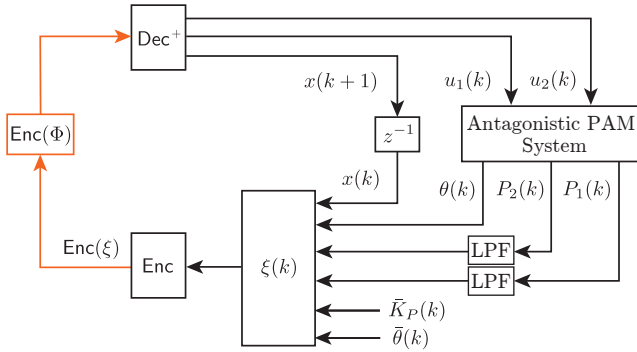


Fig. 7. Encrypted angle and stiffness control system.

chosen, and the scaling parameters  $\Delta_\xi$  and  $\Delta_\Phi$  were set to  $1.0 \times 10^8$ , which were introduced in [33] to manage the quantization errors due to encryption.

The scenarios of the control experiments involve simultaneous tracking control of the joint angle and stiffness with and without the load. The references of the joint angle and stiffness were the same as those of the simulations in Figs. 4. Before the start of the control, an initial voltage command  $u_1(0) = u_2(0) = 5.5$  was provided, and the control was initiated after sufficient time had elapsed. The experimental results are shown in Figs. 10. In the figures, the blue and green lines represent the results of the original and encrypted control systems, respectively. Figs. 9(a)(b) and 10(a)(b) confirm that the angle and stiffness track the reference in the steady state and that sufficient control performance is maintained. Similarly, they show that the controller compensated for the

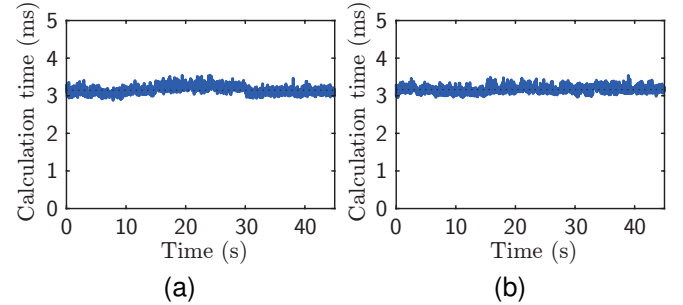


Fig. 8. Processing time: less than the sampling period of 20 ms. (a) Reference 2 without load and (b) Reference 2 with load.

impact of the load, which can be observed as a difference of approximately 50 kPa.

The computation time involved in the encrypted control system is shown in Fig. 8, where Figs. 8(a)(b) correspond to Figs. 9 and 10. The figures show that the control operation is in real time because the computation time for each step is less than the sampling period of 20 ms.

### C. Quantitative Investigation

We quantitatively evaluate the control results presented so far to investigate the impact of the secure implementation of the nonlinear controller on the control performance. For this purpose, we introduce the  $\ell_2$  norm to measure the tracking error during a specific duration for each control result, as shown in Figs. 5-6 and 9-10. The  $\ell_2$  norm is defined as  $\gamma(z, \bar{z}) := \sqrt{\sum_{k=k_0}^{k_1} (z(k) - \bar{z}(k))^2}$ , where  $z$  and  $\bar{z}$  represent scalar signal sequences, and the evaluation steps

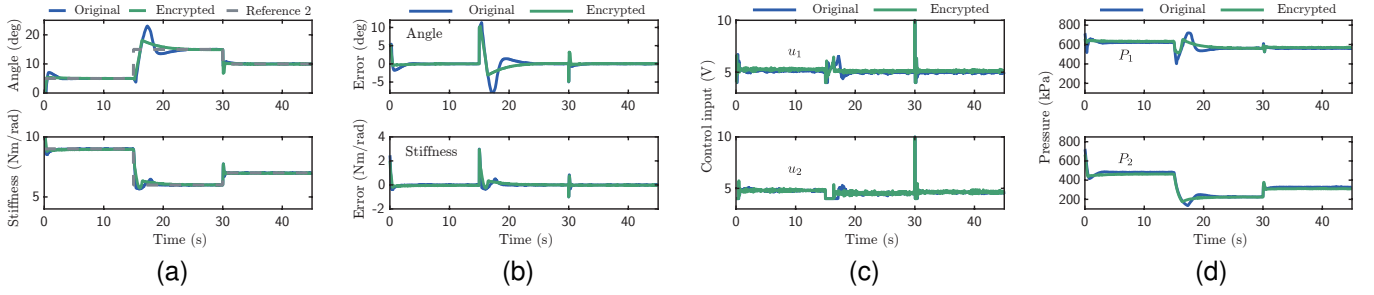


Fig. 9. Experimental results of unencrypted and encrypted simultaneous load-free control of joint angle and stiffness for Reference 2. (a) Joint angle and stiffness, (b) tracking errors of the joint angle and stiffness, (c) control inputs to the valve, and (d) inner pressure of each PAM.

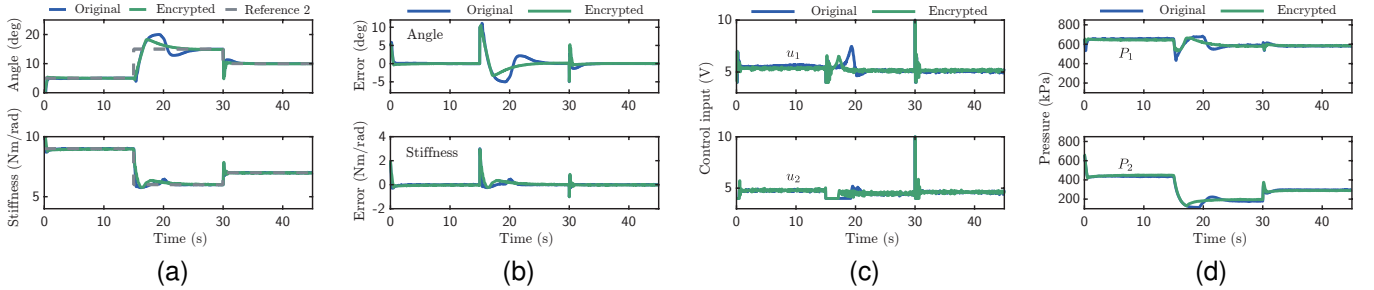


Fig. 10. Experimental results of unencrypted and encrypted simultaneous controls with load for Reference 2. (a) Joint angle and stiffness, (b) tracking errors of the joint angle and stiffness, (c) control inputs to the valve, and (d) inner pressure of each PAM.

(closed interval)  $[k_0, k_1]$  are set to  $[500, 749]$ ,  $[1250, 1499]$ , and  $[2000, 2249]$ . These intervals are labeled #1, #2, and #3, respectively, in References 1 and 2.

The  $\ell_2$ -norm scores of the original, approximated, and encrypted controls with and without loads are summarized in Figs. 11 and 12, respectively. In each figure, (a) and (b) display  $\gamma(\theta, \bar{\theta})$  and  $\gamma(K_P, \bar{K}_P)$ , respectively, for the three evaluation steps. The blue, red, and green colors represent the  $\ell_2$ -norm values of the original, approximated, and encrypted controllers, respectively. The dots and error bars indicate the average, maximum, and minimum  $\ell_2$ -norm values from 10 experiments.

These figures confirm that the resulting scores tend to increase as the procedure advances through the polynomial approximation and secure implementation. However, in many cases, the scores of the original and encrypted controllers are similar. The worst rate of the controlled signal relative to its reference is  $3.89/4.00 \times 100 = 97.3\%$  for #3 of Reference 1 in Fig. 11(b). This result implies that the proposed encrypted control achieved a tracking error of less than 2.7%. Moreover, in cases where a relatively large change in the score occurs, such as #2 of Reference 2 in Fig. 11(a) and #3 of Reference 1 in Fig. 12(b), the effect of the polynomial approximation prevails over the change in. In other words, the change in score from blue to red is larger than that from red to green. This discussion provides further insight, suggesting that increasing the accuracy of the polynomial approximation could help avoid the degradation of the original control performance. It is crucial to consider an accuracy-aware approximation method suitable for secure implementation, which will be the focus of future work. In addition, these figures confirm that, owing to

the lack of significant differences between the cases without and with the load, the proposed control system is capable of compensating for the unknown load.

## V. CONCLUSION

This study proposed an encrypted simultaneous control system for antagonistic PAM actuators aimed at developing cyber-secure and safe PAM actuator systems. A novel nonlinear controller was designed to track the joint angle and stiffness simultaneously based on the PAM actuator model. By applying the polynomial approximation technique to a nonlinear controller, we obtained a polynomial-type controller. Subsequently, through the secure implementation in the control device, we developed a secure PAM actuator system. For experimental validation, the  $\ell_2$  norm was introduced to measure and compare the experimental results of the original, approximated, and encrypted controllers. The experimental results showed that the proposed encrypted controller achieved simultaneous tracking of the joint angle and stiffness of the PAM actuator with a tracking error of less than 2.7%. Consequently, the developed PAM actuator system, enabled by the secure implementation of the simultaneous controller, enhances security while maintaining a control performance similar to that of the original controller. The developed actuator is expected to be used in secure and safe PAM-driven devices, such as nursing care robots, rehabilitation orthoses, and power-assisted orthoses for remote usage applications.

In future work, we plan to improve the control performance of the encrypted controller further by addressing the nonlinear characteristics of PAMs, including Coulomb friction and fluid dynamics. To mitigate the performance degradation caused by



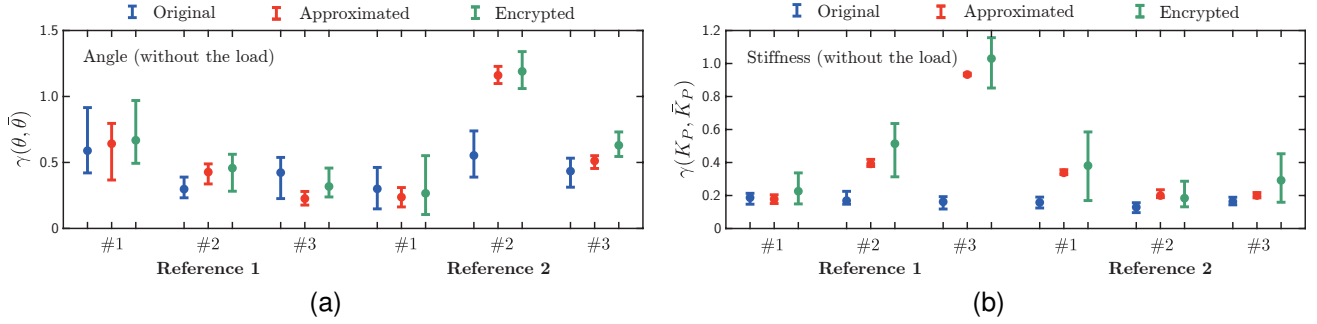


Fig. 11.  $\ell_2$ -norm scores of the tracking errors of the (a) joint angle and (b) stiffness using the original, approximated, and encrypted controllers without a load.

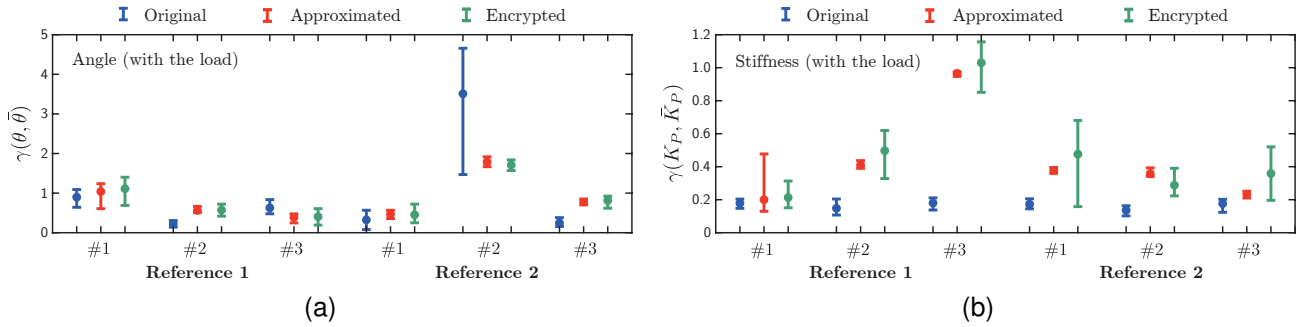


Fig. 12.  $\ell_2$ -norm scores of the tracking error of the (a) joint angle and (b) stiffness using the original, approximated, and encrypted controllers with a load.

the polynomial approximation, we investigate more effective strategies for tuning the regularization parameter in LASSO. Moreover, when considering the secure implementation of cost-effective computers, reducing the computation time is essential to achieve a resource-aware encrypted controller by streamlining the proposed controller.

## REFERENCES

- [1] Ching-Ping Chou and B. Hannaford, "Measurement and modeling of McKibben pneumatic artificial muscles," *IEEE Transactions on Robotics and Automation*, vol. 12, no. 1, pp. 90–102, 1996.
- [2] D. G. Caldwell, G. A. Medrano-Cerda, and M. Goodwin, "Control of pneumatic muscle actuators," *IEEE Control Systems Magazine*, vol. 15, no. 1, pp. 40–48, 1995.
- [3] B. Tondu and P. Lopez, "Modeling and control of McKibben artificial muscle robot actuators," *IEEE Control Systems Magazine*, vol. 20, no. 2, pp. 15–38, 2000.
- [4] T. V. Minh, B. Kamers, T. Tjahjowidodo, H. Ramon, and H. Van Brussel, "Modeling torque-angle hysteresis in a pneumatic muscle manipulator," in *IEEE/ASME International Conference on Advanced Intelligent Mechatronics*, 2010, pp. 1122–1127.
- [5] P. Beyl, K. Knaepen, S. Duerinck, M. V. Damme, B. Vanderborght, R. Meeusen, and D. Lefeber, "Safe and compliant guidance by a powered knee exoskeleton for robot-assisted rehabilitation of gait," *Advanced Robotics*, vol. 25, no. 5, pp. 513–535, 2011.
- [6] G. Andrikopoulos, G. Nikolakopoulos, and S. Manesis, "Non-linear control of pneumatic artificial muscles," in *Mediterranean Conference on Control and Automation*, 2013, pp. 729–734.
- [7] M. Tóthová and J. Pitel, "Simulation of actuator dynamics based on geometric model of pneumatic artificial muscle," in *International Symposium on Intelligent Systems and Informatics*, 2013, pp. 233–237.
- [8] G. Andrikopoulos, G. Nikolakopoulos, and S. Manesis, "Advanced non-linear PID-based antagonistic control for pneumatic muscle actuators," *IEEE Transactions on Industrial Electronics*, vol. 61, no. 12, pp. 6926–6937, 2014.
- [9] G. Andrikopoulos, G. Nikolakopoulos, and S. Manesis, "Novel considerations on static force modeling of pneumatic muscle actuators," *IEEE/ASME Transactions on Mechatronics*, vol. 21, no. 6, pp. 2647–2659, 2016.
- [10] P. K. Jamwal, S. Hussain, Y. H. Tsoi, and S. Q. Xie, "Musculoskeletal model for path generation and modification of an ankle rehabilitation robot," *IEEE Transactions on Human-Machine Systems*, vol. 50, no. 5, pp. 373–383, 2020.
- [11] D. Gong, L. Hao, J. Yu, and G. Zuo, "Bionic design of a dexterous anthropomorphic hand actuated by antagonistic PAMs," in *IEEE International Conference on Real-time Computing and Robotics*, 2020, pp. 493–498.
- [12] K. Zhou, X. Sun, R. Yu, X. Liu, and B. Wang, "Pneumatic artificial muscle antagonistic joint trajectory tracking using adaptive explicit model predictive control," in *International Conference on Computers and Automation*, 2022, pp. 48–55.
- [13] G. Andrikopoulos, G. Nikolakopoulos, and S. Manesis, "A survey on applications of pneumatic artificial muscles," in *Mediterranean Conference on Control Automation*, 2011, pp. 1439–1446.
- [14] I. Sardellitti, G. Palli, N. G. Tsagarakis, and D. G. Caldwell, "Antagonistically actuated compliant joint: Torque and stiffness control," in *IEEE/RSJ International Conference on Intelligent Robots and Systems*, 2010, pp. 1909–1914.
- [15] L. M. Sui and S. Q. Xie, "A model of pneumatic muscle actuated joint using linearized method," in *International Conference on Mechatronics and Machine Vision in Practice*, 2012, pp. 414–419.
- [16] B. Ugurlu, P. Forni, C. Doppmann, and J. Morimoto, "Torque and variable stiffness control for antagonistically driven pneumatic muscle actuators via a stable force feedback controller," in *IEEE/RSJ International Conference on Intelligent Robots and Systems*, 2015, pp. 1633–1639.
- [17] Y. Yamamoto, N. Matsunaga, and H. Okajima, "Robust variable stiffness control of McKibben type pneumatic artificial muscle arm by using multiple model error compensators," in *International Conference on Control, Automation and Systems*, 2017, pp. 957–962.
- [18] X. Zhao, H. Ma, D. Ye, and D. Zhang, "Independent stiffness and force control of antagonistic pneumatic artificial muscles joint," in *IEEE International Conference on Advanced Robotics and Mechatronics*, 2017, pp. 734–739.
- [19] D. Tanaka, H. Maeda, and T. Nakamura, "Joint stiffness and position

control of an artificial muscle manipulator considering instantaneous load,” in *Annual Conference of IEEE Industrial Electronics*, 2009, pp. 2259–2264.

- [20] T. Choi, B. Choi, and K. Seo, “Position and compliance control of a pneumatic muscle actuated manipulator for enhanced safety,” *IEEE Transactions on Control Systems Technology*, vol. 19, no. 4, pp. 832–842, 2011.
- [21] J. Cao, S. Q. Xie, and R. Das, “MIMO sliding mode controller for gait exoskeleton driven by pneumatic muscles,” *IEEE Transactions on Control Systems Technology*, vol. 26, no. 1, pp. 274–281, 2018.
- [22] N. Saito and T. Satoh, “Posture control considering joint stiffness of a robotic arm driven by rubberless artificial muscle,” *International Journal of Automation Technology*, vol. 10, no. 4, pp. 503–510, 2016.
- [23] B. Ugurlu, P. Furni, C. Doppmann, E. Sariyildiz, and J. Morimoto, “Stable control of force, position, and stiffness for robot joints powered via pneumatic muscles,” *IEEE Transactions on Industrial Informatics*, vol. 15, no. 12, pp. 6270–6279, 2019.
- [24] T. Shin and K. Kogiso, “Sensorless angle and stiffness control of antagonistic PAM actuator using reference set,” *Advanced Robotics*, vol. 36, no. 9, pp. 423–437, 2022.
- [25] H. Li, K. Tadano, and K. Kawashima, “Achieving force perception in master-slave manipulators using pneumatic artificial muscles,” in *SICE Annual Conference*, 2012, pp. 1342–1345.
- [26] T. Sasaki, T. Nagai, and K. Kawashima, “Remote control of backhoe for rescue activities using pneumatic robot system,” in *IEEE International Conference on Robotics and Automation*, 2006, pp. 3177–3182.
- [27] T. Kato, T. Higashi, and K. Shimizu, “Teleoperation of a robot arm system using pneumatic artificial rubber muscles: Teleoperation over the internet using udp and a web camera,” in *International Conference on Broadband, Wireless Computing, Communication and Applications*, 2010, pp. 714–718.
- [28] H. Toda, M. Tada, T. Maruyama, and Y. Kurita, “Effect of contraction parameters on swing support during walking using wireless pneumatic artificial muscle driver: A preliminary study,” in *Annual Conference of the Society of Instrument and Control Engineers*, 2019, pp. 727–732.
- [29] S. Yean, M. Tada, H. Toda, B.-S. Lee, and Y. Kurita, “Adaptive automatic controller for swing assist by pneumatic artificial muscle,” in *IEEE Sensors Applications Symposium*, 2020, pp. 1–6.
- [30] R. Langner, “Stuxnet: Dissecting a cyberwarfare weapon,” *IEEE Security & Privacy*, vol. 9, no. 3, pp. 49–51, 2011.
- [31] S. Gorman, Y. J. Dreazen, and Cole, “Insurgents hack US drones,” <https://www.wsj.com/articles/SB126102247889095011>, 2009.
- [32] D. Quarta, M. Pogliani, M. Polino, F. Maggi, A. M. Zanchettin, and S. Zanero, “An experimental security analysis of an industrial robot controller,” in *IEEE Symposium on Security and Privacy*, 2017, pp. 268–286.
- [33] K. Kogiso and T. Fujita, “Cyber-security enhancement of networked control systems using homomorphic encryption,” in *IEEE Conference on Decision and Control*, 2015, pp. 6836–6843.
- [34] K. Teranishi, K. Kogiso, and J. Ueda, “Encrypted feedback linearization and motion control for manipulator with somewhat homomorphic encryption,” in *IEEE/ASME International Conference on Advanced Intelligent Mechatronics*, 2020, pp. 613–618.
- [35] Y. Qiu and J. Ueda, “Encrypted motion control of a teleoperation system with security-enhanced controller by deception,” in *Dynamic Systems and Control Conference*, vol. 59148, 2019, p. V001T07A006.
- [36] T. Shin, K. Teranishi, and K. Kogiso, “Cyber-secure pneumatic actuator system equipped with encrypted controller and attack detectors,” *Advanced Robotics*, vol. 36, no. 9, pp. 438–449, 2022.
- [37] R. Baba, K. Kogiso, and M. Kishida, “Detection method of controller falsification attacks against encrypted control system,” in *SICE Annual Conference*, 2018, pp. 244–248.
- [38] M. Miyamoto, K. Teranishi, K. Emura, and K. Kogiso, “Cybersecurity-enhanced encrypted control system using keyed-homomorphic public key encryption,” *IEEE Access*, vol. 11, pp. 45 749–45 760, 2023.
- [39] M. Schulze Darup, “Encrypted polynomial control based on tailored two-party computation,” *International Journal of Robust and Nonlinear Control*, vol. 30, no. 11, pp. 4168–4187, 2020.
- [40] T. Shin, T. Ibayashi, and K. Kogiso, “Detailed dynamic model of antagonistic PAM system and its experimental validation: Sensorless angle and torque control with UKF,” *IEEE/ASME Transactions on Mechatronics*, vol. 27, no. 3, pp. 1715–1726, 2022.
- [41] Y. Takeda and K. Kogiso, “Experimental regularization parameter search for polynomial approximation of nonlinear PAM controller,” in *IEEE/SICE International Symposium on System Integration*, 2023, pp. 963–968.



**Yuta Takeda** received the B.S. degree in Informatics and Engineering from The University of Electro-Communications, Tokyo, Japan, in 2022. He is currently an M.S. student at The University of Electro-Communications, Tokyo, Japan.

His research interests include control applications and modeling/control of pneumatic artificial muscles.



**Takaya Shin** received the B.S. and M.S. degrees in Informatics and Engineering from The University of Electro-Communications, Tokyo, Japan, in 2020 and 2022, respectively. He joined Daihen Co., Osaka, Japan.

His research interests include control applications and modeling/control of pneumatic artificial muscles.



**Kaoru Teranishi** received the B.S. degree in electromechanical engineering from National Institute of Technology, Ishikawa College, Ishikawa, Japan, in 2019. He also obtained the M.S. degree in Mechanical and Intelligent Systems Engineering from The University of Electro-Communications, Tokyo, Japan, in 2021. He is currently a Ph.D. student at The University of Electro-Communications. From October 2019 to September 2020, he was a visiting scholar of the Georgia Institute of Technology, GA, USA. Since April 2021, he has been a Research

Fellow of the Japan Society for the Promotion of Science. His research interests include control theory and cryptography for cyber-security of control systems.



**Kiminao Kogiso** received the B.E., M.E., and Ph.D. degrees in mechanical engineering from Osaka University, Japan, in 1999, 2001, and 2004, respectively. He was appointed a postdoctoral fellow in the 21st Century COE Program and as an Assistant Professor in the Graduate School of Information Science, Nara Institute of Science and Technology, Nara, Japan, in April 2004 and July 2005, respectively. From November 2010 to December 2011, he was a visiting scholar at the Georgia Institute of Technology, GA, USA. In March 2014, he was promoted to associate

professor in the Department of Mechanical and Intelligent Systems Engineering at The University of Electro-Communications, Tokyo, Japan. Since April 2023, he has been a professor in the same department. His research interests include the cybersecurity of control systems, constrained control, control of decision-makers, and their applications.